DEUTSCHES ELEKTRONEN-SYNCHROTRON DESY

DESY 90–098
August 1990

W, Z plus Jet Production at $p\bar{p}$ Colliders

F.T. Brandt, G. Kramer, Su-Long Nyeo
II. Institut für Theoretische Physik, Universität Hamburg

ISSN 0418-9833

NOTKESTRASSE 85 · 2 HAMBURG 52

To be sure that your preprints are promptly included in the
HIGH ENERGY PHYSICS INDEX ,
send them to the following address (if possible by air mail) :

DESY
Bibliothek
Notkestrasse 85
2 Hamburg 52
Germany

DESY 90-098
August 1990

ISSN 0418-9833

W, Z plus Jet Production at $p\bar{p}$ Colliders

F.T. Brandt *, G. Kramer, Su-Long Nyeo +

II. Institut für Theoretische Physik, Universität Hamburg,
Luruper Chaussee 149, D-2000 Hamburg 50, FRG

* Present address: Instituto de Física, Universidade de São Paulo, CX. Postal 20516,
01498 - São Paulo, SP, Brazil

+ Present address: Institute of Physics, Academia Sinica, Taipei 11529, Taiwan, R.O.C

Abstract:

We have calculated cross sections for the production of $W^{\pm}$ and Z bosons in association with 1 and 2 jets at $p\bar{p}$ collider energies. The rates for these processes in second-order QCD are compared with jet rates measured by UA1 and CDF.

1. Introduction

The production of weak bosons with hadronic jets is an important process to provide further tests of perturbative QCD at large momentum transfer. Experimental data for jet production rates f_n for W production and n = 0, 1, 2, 3, 4 and for Z production and n = 0, 1, 2, 3 have been presented recently by the UA1 [1] and UA2 [2] collaborations at CERN's $p\bar{p}$ collider and the CDF collaboration [3, 4] at FERMILAB's Tevatron. For the Tevatron energy also preliminary data of the transverse momentum distribution of the produced W in association with one or two hadron jets have become available [3].

Some months ago we completed a theoretical evaluation of jet cross sections for W and Z production associated with one or two additional jets (the projectile remnants are not counted as jets) based on perturbative QCD up to order α_s^2 [5]. We studied the transverse momentum distributions of the weak bosons for the one- and two-jet sample with various cuts p^j_{Tmin} of the jets and calculated the jet fractions f_n (n = 1, 2) from them. These predictions of jet cross sections in association with W and Z production have different theoretical qualifications. In $O(\alpha_s^2)$ the 2-jet cross section can come only from tree diagrams. Therefore this cross section depends strongly on the choice of the factorization and renormalization mass scales. The 1-jet cross section, on the other hand, which is calculated up to $O(\alpha_s^2)$, receives contributions from tree diagrams up to $O(\alpha_s^2)$ and from $O(\alpha_s^2)$ virtual diagrams which require renormalization. Therefore this cross section depends much less on the factorization and renormalization scales; changes of scales in the parton distribution or the strong coupling α_s are compensated by changes of higher order corrections. Thus, the prediction for the 1-jet cross section is much more meaningful from the theoretical point of view than tree level results [6] which are so far available for the higher jet classes n = 2 and 3. The same is true for the zero-jet cross section, which is the cross section for W, Z production with no extra hadron jet. This can be calculated from the total W, Z production cross section by subtracting the 1-jet and 2-jet cross sections. The calculation of the total W, Z production cross section up to $O(\alpha_s^2)$ has been completed recently [7]. In this way also the zero-jet cross section is known up to $O(\alpha_s^2)$ which now has also a reduced factorization and renormalization scale dependence similar to the 1-jet cross section.

Of course, to make theoretical predictions for W, Z production in the framework of perturbative QCD we need the parton densities of the projectiles. These densities come from deep-inelastic lepton-nucleon scattering data. We shall employ the recently published parton distributions of Harriman, Martin, Stirling and Roberts (HMSR) [8]. They have been derived from a next-to-leading order structure function analysis of deep-inelastic muon and neutrino scattering data with $\overline{MS}$ renormalization description. In particular, they incorporated new $F_2^{\mu n}/F_2^{\mu p}$ data and took account of a recent re-analysis of SLAC data. In addition their fit is performed simultaneously with next-to-leading-order fits to prompt photon and Drell-Yan data. For the μ-p structure function $F_2^{\mu p}$ they used, as in their earlier analysis, the EMC and BCDMS measurements. Due to the fact that these data sets do not overlap fully, they extracted again two sets of parton distribution functions, according to whether the EMC or BCDMS muon data are included in the fit, called set HMRS (E) and set HMRS (B) respectively. Furthermore they performed a global renormalization of the EMC and BCDMS data by comparison with the SLAC data which brought these two data sets nearer together. These new parton distributions supersede the sets MRS EB mode 1 and 2 used in our earlier work [5].

The purpose of this paper is twofold. First due to the fact that the complete W, Z production cross sections have been calculated up to $O(\alpha_s^2)$ we can obtain fully-normalized p_T distributions for the inclusive cross section, i.e. the sum of 1- and 2-jet cross sections, and for the 1- and 2-jet cross sections separately. With these cross sections, we can do also for the corresponding jet rates which allows us to derive also the zero-jet fraction. Second we want to compare with new experimental data, which were published recently [3, 4] and which allow us a more meaningful test of the QCD predictions than in [5]. The input of our calculations is the same as in our earlier work. The results of the inclusive (1+2)-jet cross section up to $O(\alpha_s^2)$ are obtained as in [5] from the work of Gonsalves et al. [9]. The definition of cuts to define 1- and 2-jet cross sections is fully described in [5]. However, we changed the structure function input as described above. In the next section we present our results at $\sqrt{S}$ = 0.63 and 1.8 TeV, respectively, and compare them to experimental data for the cases where they are available. Furthermore we show some results at $\sqrt{S}$ = 16 and 40 TeV.

2. Results

A. Inclusive Cross Sections

First we present the inclusive (1+2)-jet cross section normalized with the total cross section as evaluated in [7]. For comparison with data we do this for the CERN collider energy $\sqrt{S}$ = 0.63 TeV (only W production) and the Tevatron energy $\sqrt{S}$ = 1.8 TeV (W and Z production). For W production we have added the cross section for W^+ and W^- production as was done in the measurements. The coupling α_s is calculated with $\Lambda_{\overline{MS}}$ = 0.1 GeV for the case that we use the HMRS (E) set of parton densities and $\Lambda_{\overline{MS}}$ = 0.19 GeV for the HMRS (B) set from the functional form given in [10]. We use M_W = 80.27 GeV and M_Z = 91.17 GeV. The total cross section is also calculated with these two sets of parton densities and $\Lambda_{\overline{MS}}$ [7]. For W and Z production the results are given and Table 1a, b as σ^0 (lowest order cross section), σ^1 (up to $O(\alpha_s)$) and σ^2 (up to $O(\alpha_s^2)$) for the HMRS (E) and the HMRS (B) set. The $O(\alpha_s^2)$ contribution was evaluated with the help of [7], but with the new parton densities [8] and the $\overline{MS}$ factorization scheme [11]. We see that the two sets give almost equal W and Z cross sections at $\sqrt{S}$ = 0.63 TeV. At $\sqrt{S}$ = 1.8 TeV the cross sections with set B are 8% and 6% larger than the cross sections with

set E for W and Z production respectively. This difference increases with increasing $\sqrt{S}$. At $\sqrt{S}$ = 40 TeV the predictions of the total cross section for W and Z production differ appreciably. For example, the W cross section with set B and the corresponding $\Lambda_{\overline{MS}}$ is 53% larger than the cross section with set E. The reason for this is quite clear. For the lower energies the momentum fractions x_i (i = 1, 2) that are probed lie within the range of x of the data fitted in the global structure function analysis, i.e. $x \gtrsim 0.03$. The proposed LHC and SSC colliders with energies $\sqrt{S}$ = 16 TeV and $\sqrt{S}$ = 40 TeV test much smaller x values in such regions where the parton distributions are not constrained by the deep inelastic scattering data. Actually for these small x regions other structure function sets are conceivable, in particular for the assumed gluon structure function at low Q^2, and lead to W, Z cross sections that vary by up to a factor 3 (at $\sqrt{S}$ = 40 TeV) depending on the assumed set of parton distributions [12]. At these high collider energies the contribution from valence-valence scattering is very small and therefore $\sigma_{W,Z}(pp) \simeq \sigma_{W,Z}(p\bar{p})$. The results for p+p → W,Z+X at $\sqrt{S}$ = 16 and 40 TeV are given in Table 1a, b in parentheses.

The inclusive p_T distributions are shown in Fig. 1 (W production, $\sqrt{S}$ = 0.63 TeV), Fig. 2 (W production, $\sqrt{S}$ = 1.8 TeV) and Fig. 3 (Z production, $\sqrt{S}$ = 1.8 TeV). We see that these distributions, which are normalized with σ from Table 1a, b, depend very little on the structure function set. The curves for $\sqrt{S}$ = 0.63 TeV are compared with recent data of the UA2 collaboration [13]. The data are plotted only for $p_T^W > 20$ GeV. The agreement is very good. The W and the Z p_T spectra at $\sqrt{S}$ = 1.8 TeV are compared with recent CDF data [3, 4] in Fig. 2 and 3. These data are preliminary and need some correction work, although the acceptance/efficiency correction had been applied. The agreement between data and the theoretical prediction is more than four decades. This shows that the energy dependence of these W and Z spectra between 0.63 and 1.8 TeV is very well reproduced with no adjustments of the normalization needed. To get an idea on how the theoretical predictions look like at much higher energies we have computed $^1/_\sigma \, d\sigma/dp_T$ for W production at $\sqrt{S}$ = 16 TeV and $\sqrt{S}$ = 40 TeV for $p\bar{p}$ and pp collisions and both sets of parton distributions. The results are presented in Fig. 4. The difference of the two sets shows up only at large p_T above 0.5 TeV. The predictions for $p\bar{p}$ and pp approach each other with increasing energy, since for large S the contributions of the valence distributions become negligible.

With more data coming from the CDF experiment it may be possible to obtain the cross section for W^+ and W^- production separately. These two cross sections differ in their rapidity dependence. Since $\sigma_{W^+}(y) = \sigma_{W^-}(-y)$ it is sufficient to consider the production of W^+ over the complete rapidity range. Then the asymmetry between the cross section of $y > 0$ and $y < 0$ is more sensitive to details of the structure functions than the over y integrated cross section which is equal for W^+ and W^- production. In Fig. 5 we show that differential distribution $\left(^1/\sigma_{W^+}\right) d^2\sigma_{W^+}/dp_T dy$ as a function of p_T of the W^+ for various y = 0.0, 1.0, 1.5, -1.0 and -1.5, at $\sqrt{S}$ = 0.63 TeV for the HMRS (E) set. As we

can see these p_T distributions are not symmetric for y → -y. To obtain the corresponding distributions for W^- production one must transform y → -y. The same results at $\sqrt{S}$ = 1.8 TeV and for the HMRS (E) set are plotted in Fig. 6 and 7. In Fig. 6 we show the results for positive y = 0.0, 1.0, 1.5, 2.0 and 2.5 and in Fig. 7 the results for the corresponding negative rapidity values. As to be expected the cross sections are largest for y = 0 and decrease with increasing |y|. The double-differential distributions for the HMRS (B) set look similar; the results for both sets differ on average by 10% for $\sqrt{S}$ = 0.63 TeV and by 20% for $\sqrt{S}$ = 1.8 TeV.

B. Jet Cross Sections

To obtain the cross section for one or two associated jets we took the same route as in [5]. We calculated the 2-jet cross section from the complete list of tree diagrams in $O(\alpha_s^2)$ with the appropriate cuts. Then this cross section is subtracted from the inclusive (1+2)-jet cross section considered in section A. This gives the 1-jet cross section. For $\sqrt{S}$ = 0.63 GeV we defined the cuts as $p_T^j \geq 10$ GeV, $\Delta R \geq 1.0$ and $|\eta| \leq 2.5$. Except for the cut on the transverse jet momentum p_T^j these are the same cuts as in the UA1 experiment [2]. For $\sqrt{S}$ = 1.8 TeV we employ the cuts $p_T^j \geq 15$ GeV, $\Delta R \geq 0.7$ and $|\eta| \leq 2.2$ to agree with the CDF resolution cuts [3, 4]. The p_T^W distributions of the 1-jet and 2-jet contributions at $\sqrt{S}$ = 1.8 TeV are exhibited in Fig. 8 (1-jet) and Fig. 9 (2-jet) and compared to recent CDF data [3]. The data are still uncorrected. Therefore the comparison has only qualitative significance. The normalization of the data is not known. Therefore only the shape of the curves can be compared. However, the rather steep fall-off of the 1-jet distribution and the flat behaviour of the 2-jet distribution is born out in the data. The 1- and 2-jet Z production cross sections show the same behaviour as a function of p_T^Z as is seen in Fig. 10. The theoretical curves are for both sets of parton densities. They differ very little. Their difference is approximately the same as in the total cross sections (see Table 1a, b). We have integrated the distribution in Fig. 8, 9 and 10 over p_T^W and p_T^Z respectively down to some minimum value p_T^{min} ranging between 5.0 GeV and 30 GeV. The results are given in the form of tables. In Table 2a, b we have collected the zero-jet fraction σ_0/σ, the one-jet fraction σ_1/σ and the two-jet fraction σ_2/σ for W and Z production, respectively for $\sqrt{S}$ = 1.8 TeV. From these tables we can read off the jet rates f_0, f_1 and $f_{2'}$ for which $p_{T\,min}^j = p_T^{min}$ = 15 GeV, where p_T^{min} is the cut on the p_T^W or p_T^Z. The average values for the two sets E and B are compared to preliminary CDF data in Fig. 11a (W+n-jet fraction) and Fig. 11b (Z+n-jet fraction) [3]. The Z+n jet fractions (n = 0, 1, 2) agree with the data inside the experimental errors. In the case of the W+n-jet fraction f_2 is 50% lower than the measured value. Whether this is significant and signals that in the 2-jet fraction higher order corrections of $O(\alpha_s^3)$ are important is unclear in the moment. Similar, even larger discrepancies have been observed for the 4-jet rate in e^+e^- annihilation [14] which comes also from tree diagrams in $O(\alpha_s^2)$. We shall come back to this point in section C.

Jet fractions σ_0/σ, σ_1/σ and σ_2/σ for $\sqrt{S}$ = 0.63 TeV with cuts $p_T^j \geq 10$ GeV, $\Delta R \geq 1.0$ and $|\eta| < 2.5$, to be of interest for future analysis of UA1 and UA2 data are collected in Table 3a and b with p_T^W and p_T^Z varying between 5.0 and 20 GeV. These results can not be used for a comparison with UA1 data [2] on jet fractions f_n (n = 0, 1, 2) for W and Z production with a cut of 5 GeV on the jet transverse momentum. We compared these data: $f_0 = 0.63 \pm 0.05$, $f_1 = 0.29 \pm 0.05$, $f_2 = 0.065 \pm 0.015$ for W production and $f_0 = 0.56 \pm 0.12$, $f_1 = 0.33 \pm 0.07$, $f_2 = 0.092 \pm 0.046$ with our results obtained in [5]. Since σ up to $O(\alpha_s^2)$ was not known at that time we could compare only the ratios f_1/f_0 and f_2/f_0 with the theory, assuming that σ_0 is not changed by higher order corrections. We have rerun this case ($p_T^j \geq 5$ GeV) with the new structure functions. Taking these new results we obtained for the W+n-jet fractions, f_0 = 0.66 (0.65), f_1 = 0.29 (0.30), f_2 0.044 (0.049), and for Z+n-jet fractions f_0 = 0.64 (0.62), f_1 = 0.30 (0.31), f_2 = 0.061 (0.064) for set E(B). The numbers agree nicely with the UA1 data inside errors given above. Unfortunately the experimental errors are still large so that it is not possible to detect any discrepancy in f_2 as we noticed for f_2 at $\sqrt{S}$ = 1.8 TeV in the case of W production.

C. Scale Dependence of Jet Fractions

The next-to-leading-order cross sections depend on the choice of renormalization and factorization schemes and scales. We use the $\overline{MS}$ factorization scheme appropriate to the HMRS parton densities [8]. Within this factorization scheme we have still the freedom to choose the factorization scale M. We have chosen $M = M_W$ and M_Z for W and Z production, respectively. The dependence on M has been investigated for σ_{tot} in [7] and for the inclusive p_T distribution in [9] with the result that the factorization scale dependence is rather weak. Of course, it would be worthwhile to study this in more detail. In this section we shall look into the renormalization scheme dependence μ. The motivation for this is that above we noted that the 2-jet rate for W production disagrees with the CDF data by more than 50%. This disagreement may come from different sources: i) the data are preliminary and may change after all experimental corrections have been applied, ii) fragmentation effect were left out in the calculation of the 2-jet rate at $O(\alpha_s^2)$, iii) lowest order perturbation theory is not sufficient to predict the 2-jet rate. Although i) and ii) are not excluded we shall look only into the possibility iii). Of course, we shall not be able to obtain results beyond second order in α_s. Instead we study the renormalization scale dependence $\mu^2 = fQ^2$ of the jet fractions σ_0/σ, σ_1/σ, σ_2/σ and of σ, hoping that σ, σ_0/σ and σ_1/σ which have higher order corrections are only moderately dependent on μ^2 (or f), whereas σ_2/σ, which comes from tree graphs only, will depend strongly on μ^2. If we reduce μ^2 compared to $\mu^2 = Q^2$ the 2-jet fraction will increase. By adjusting μ^2 it will be possible to fit the experimental number for σ_2/σ. Then the question arises as to whether σ and σ_1/σ are still in agreement with the data [3, 4]. To make this test we have calculated σ_0/σ, σ_1/σ, σ_2/σ and σ as a function of f after transforming $\alpha_s(Q^2)$ into $\alpha_s(fQ^2)$ with the well-known formula which relates α_s at two different scales [15]. The results for W+n-jet and Z+n-jet production are shown in Fig. 12 for the $\sqrt{S}$ =

0.63 TeV, $p_T^j \geq 5$ GeV jet fractions and σ, respectively, and in Fig. 13 for the $\sqrt{S}$ = 1.8 TeV, $p_T^j \geq 15$ GeV jet fractions and σ. We have chosen N_f = 5, $\Lambda_{\overline{MS}}$ = 0.1 GeV and set E. As to be expected, σ_2/σ is a monotonic function of f and increases strongly with decreasing f. σ_0/σ and σ_1/σ and σ itself are only moderately dependent on f. To fit the W+2-jet rate $\sigma_2/\sigma = 0.3$ as was experimentally measured (see Fig. 11a) we need $f = 3 \cdot 10^{-2}$. For this scale we have σ = 18.77 nb compared to σ = 18.16 nb at f = 1 and σ_1/σ = 0.19 and σ_0/σ = 0.78 which are still compatible with the data in Fig. 11a. We conclude from this that by adjusting the renormalization scale f it might be possible to get agreement for all three jet fractions in W+n-jet production at $\sqrt{S}$ = 1.8 TeV with the data of CDF [3, 4]. Similar adjustments of the renormalization scale have been performed for jet fractions in e^+e^- annihilations in order to fit the 4-jet rate [14, 15], which is also obtained from $O(\alpha_s^2)$ tree diagrams. Whereas there is no physical significance in the obtained scale, its variation apparently allows a better description of all jet fractions up to $O(\alpha_s^2)$ and, in this way, accounts for deficiencies originating from neglecting higher orders in QCD perturbation theory.

Acknowledgements: F.T. Brandt and S.-L. Nyeo would like to thank the Alexander-von-Humboldt Foundation for fellowships. We are grateful to W.J. Stirling for sending us computer codes of the HMRS parton densities and to T. Matsuura for calculating the $O(\alpha_s^2)$ contribution to the total cross section with the HMRS densities.

Table Captions:

Table 1a: The total cross section for $W^+ + W^-$-production at $Sp\bar{p}S$, Tevatron, LHC and SSC energies in lowest order (σ^0), up to $O(\alpha_s)$ (σ^1) and up to $O(\alpha_s^2)$ (σ^2) for structure function sets HMRS (E) and HMRS (B). Numbers in brackets are for pp collisions.

Table 1b: Same as Table 1a, but for Z production.

Table 2a: W+n-jet rates (n = 0, 1, 2) for $\sqrt{S}$ = 1.8 TeV and cut on the jet transverse momentum $p_T^j \geq 15$ GeV integrated over p_T of W with lower limit p_T^{min} between 5 and 30 GeV using structure function sets E and B.

Table 2b: Z+n-jet rates (n = 0, 1, 2) for $\sqrt{S}$ 1.8 TeV for various p_T^{min} of Z and cuts as in Table 2a.

Table 3a: W+n-jet rates (n = 0, 1, 2) for $\sqrt{S}$ = 0.63 TeV and cut $p_T^j \geq 10$ GeV, integrated over p_T of W with lower limit p_T^{min} between 5 and 20 GeV for structure function sets E and B.

Table 3b: Same as Table 3a, Z+n-jet rates (n = 0, 1, 2).

Figure Captions:

Fig. 1: Inclusive transverse momentum distribution for W production at $\sqrt{S}$ = 0.63 TeV as a function of p_T^W for set E (solid line) and set B (dotted line) compared to UA2 data [13].

Fig. 2: Inclusive transverse momentum distribution for W production at $\sqrt{S}$ = 1.8 TeV as a function of p_T^W for set E (solid line) and set B (dotted line) compared to preliminary CDF data [3, 4].

Fig. 3: Same as Fig. 2, but for Z production.

Fig. 4: Inclusive transverse momentum distribution for W production at $\sqrt{S}$ = 16 TeV and $\sqrt{S}$ = 40 TeV for $p\bar{p}$ and pp collisions and sets E and B. Solid line is for pp and set E, dotted line is for pp and set B, dashed line is $p\bar{p}$ and set E, dot-dashes line is $p\bar{p}$ and set B.

Fig. 5: Double-differential distribution $d^2\sigma/dp_T dy$ as a function of p_T of W^+ for various y values: y = 0.0 (solid), y = 1.0 (dashed), y = 1.5 (dot-dashed), y = -1.0 (square dots) and y = -1.5 (triangle dots) at $\sqrt{S}$ = 0.63 TeV and set E, normalized to σ_{W^+} = 3.456 nb.

Fig. 6: Same as Fig. 5 at $\sqrt{S}$ = 1.8 TeV for positive rapidities y = 0.0 (solid), y = 1.0 (dotted), y = 1.5 (dashed), y = 2.0 (dot-dashed) and y = 2.5 (dots) and for set E, normalized to σ_{W^+} = 9.080 nb.

Fig. 7: Same as Fig. 6, for negative rapidities y = 0.0 (solid), y = -1.0 (dotted), y = -1.5 (dashed), y = -2.0 (dot-dashed) and y = -2.5 (dots).

Fig. 8: The $O(\alpha_s) + O(\alpha_s^2)$ W+1-jet transverse momentum distribution as a function of p_T^W with cut on $p_T^j \geq 15$ GeV at $\sqrt{S}$ = 1.8 TeV compared to preliminary CDF data [3], solid (dotted) line is for set E (B).

Fig. 9: W+2-jet compared to CDF data [3], $p_T^j \geq 15$ GeV, solid (dotted) line is for set E (B).

Fig. 10: Z+1-jet and Z+2-jet production as a function of p_T^Z at $\sqrt{S}$ = 1.8 TeV and $p_T^j \geq 15$ GeV, solid (dotted) line is for set E (B).

Fig. 11a: W+n-jet rates (n = 0, 1, 2) with $p_T^j \geq 15$ GeV, $|\eta| \leq 2.2$, $\Delta R \geq 0.7$ compared to preliminary CDF data [3, 4]. The crosses are the predictions.

Fig. 11b: Z+n-jet rates (n = 0, 1, 2) compared to preliminary CDF data [3, 4]. The crosses are the predictions.

Fig. 12: W, Z+n-jet rates (n = 0, 1, 2) and σ as a function of renormalization scale $f = \mu^2/Q^2$ for $\sqrt{S}$ = 0.63 TeV and $p_T^j \geq 5$ GeV.

Fig. 13: Same as Fig. 12, but for $\sqrt{S}$ = 1.8 TeV and $p_T^j \geq 15$ GeV.

References:

[1] R. Ansari et al., UA2 Collaboration, Phys. Lett. *B215* (1988) 175 and
K. Jacobs, Dissertation, University of Heidelberg, 1988, (unpublished)

[2] C. Albajar et al., UA1 Collaboration, Z. Phys. *C44* (1989) 15

[3] T. Kamon (presenting the CDF Collaboration)
FERMILAB-Conf-89/246E [E 741/CDF], to be published in the proceedings of the 8th Topical workshop on $p\bar{p}$ Collider Physics, Castiglione della Pescaia, Italy

[4] H. Grassmann (presenting the CDF collaboration), talk given at the Les Rencontres de Physique de la Vallee d'Aoste, La Thuile, Aosta Valley, France, March 18-24, 1990

[5] F.T. Brandt, G. Kramer, S.-L. Nyeo, DESY-report, DESY 90-042 and
Z. Phys. *C* (to be published)

[6] V. Barger et al., Phys. Rev. Lett. *62* (1989); Phys. Rev. *D40* (1989) 2888;
F.A. Behrends et al., Phys. Lett. *B224* (1989) 237

[7] T. Matsuura, R. Hamberg, W.L. van Neerven, DESY-report, DESY 90-031, 1990 (unpublished)

[8] P.N. Harriman, A.D. Martin, W.J. Stirling, R.G. Roberts,
Rutherford Appleton Laboratory preprint, RAL-90-007 (unpublished)

[9] R.J. Gonsalves, J. Pawlowski, C.-F. Wai, Phys. Rev. *D40* (1989) 2245; see also
P.B. Arnold, M.H. Reno, Nucl. Phys. *B319* (1989) 37

[10] Review of Particle Properties, Phys. Lett. *B204* (1988) 96

[11] T. Matsuura, private communication

[12] A.D. Martin, W.J. Stirling, University of Durham preprint,
DTP/90/34 (unpublished)

[13] J. Alitti et al., UA2 Collaboration, CERN-EP-90-52, 1990 and
Z. Phys. *C* (to be published)

[14] M.Z. Abrawy et al., Phys. Lett. *B235* (1990) 289
and the earlier references given therein.

[15] G. Kramer, B. Lampe, Z. Phys. *C39* (1988) 101

Table 1a

W Production [nb]		HMRS (E)	HMRS (B)
$\sqrt{S} = 0.63\ TeV$	σ^0	5.062	4.793
	σ^1	6.468	6.312
	σ^2	6.913	6.831
$\sqrt{S} = 1.8\ TeV$	σ^0	14.45	15.11
	σ^1	17.04	18.22
	σ^2	18.16	19.67
$\sqrt{S} = 16\ TeV$	σ^0	77.08 (75.68)	105.2 (103.8)
	σ^1	83.48 (81.79)	115.6 (113.8)
	σ^2	90.39 (88.64)	126.9 (125.1)
$\sqrt{S} = 40\ TeV$	σ^0	151.3 (150.5)	225.8 (224.8)
	σ^1	161.8 (160.8)	244.9 (243.6)
	σ^2	176.4 (175.3)	270.5 (269.2)

Table 1b

Z Production [nb]		HMRS (E)	HMRS (B)
$\sqrt{S} = 0.63\ TeV$	σ^0	1.534	1.467
	σ^1	1.966	1.939
	σ^2	2.095	2.090
$\sqrt{S} = 1.8\ TeV$	σ^0	4.474	4.592
	σ^1	5.322	5.583
	σ^2	5.660	6.009
$\sqrt{S} = 16\ TeV$	σ^0	24.14 (23.53)	32.35 (31.77)
	σ^1	26.19 (25.46)	35.60 (34.89)
	σ^2	28.33 (27.57)	39.04 (38.29)
$\sqrt{S} = 40\ TeV$	σ^0	47.81 (47.42)	70.30 (69.88)
	σ^1	51.16 (50.68)	76.28 (75.76)
	σ^2	55.79 (55.30)	84.26 (83.71)

$W + n-jet$ Production						
$p_T^{min}[GeV]$	σ_0/σ		σ_1/σ		σ_2/σ	
	E	B	E	B	E	B
5	0.465	0.445	0.514	0.534	0.0205	0.0211
10	0.692	0.683	0.288	0.297	0.0196	0.0201
15	0.802	0.800	0.180	0.181	0.0183	0.0188
20	0.864	0.865	0.119	0.118	0.0168	0.0172
25	0.903	0.905	0.0815	0.0797	0.0152	0.0156
30	0.930	0.931	0.0568	0.0549	0.0135	0.0138

Table 2a

$Z + n-jet$ Production						
$p_T^{min}[GeV]$	σ_0/σ		σ_1/σ		σ_2/σ	
	E	B	E	B	E	B
5	0.461	0.428	0.514	0.546	0.0251	0.0265
10	0.688	0.670	0.288	0.305	0.0240	0.0253
15	0.797	0.789	0.181	0.187	0.0226	0.0238
20	0.859	0.856	0.120	0.122	0.0210	0.0221
25	0.899	0.897	0.0821	0.0826	0.0192	0.0203
30	0.925	0.925	0.0578	0.0570	0.0172	0.0182

Table 2b

$W + n-jet$ Production						
$p_T^{min}[GeV]$	σ_0/σ		σ_1/σ		σ_2/σ	
	E	B	E	B	E	B
5.0	0.664	0.652	0.325	0.337	0.0106	0.0113
7.5	0.780	0.773	0.210	0.216	0.0102	0.0108
10.0	0.846	0.843	0.144	0.147	0.00961	0.0102
12.5	0.889	0.886	0.102	0.104	0.00900	0.00956
15.0	0.918	0.916	0.0741	0.0751	0.00834	0.00885
17.5	0.938	0.937	0.0546	0.0551	0.00762	0.00807
20.0	0.952	0.952	0.0409	0.0411	0.00680	0.00721

Table 3a

$Z + n-jet$ Production						
$p_T^{min}[GeV]$	σ_0/σ		σ_1/σ		σ_2/σ	
	E	B	E	B	E	B
5.0	0.640	0.624	0.345	0.360	0.0154	0.0159
7.5	0.759	0.751	0.226	0.234	0.0148	0.0153
10.0	0.830	0.824	0.156	0.161	0.0141	0.0145
12.5	0.875	0.872	0.112	0.114	0.0133	0.0137
15.0	0.906	0.904	0.0818	0.0831	0.0124	0.0128
17.5	0.928	0.927	0.0608	0.0611	0.0114	0.0118
20.0	0.944	0.944	0.0459	0.0456	0.0103	0.0106

Table 3b

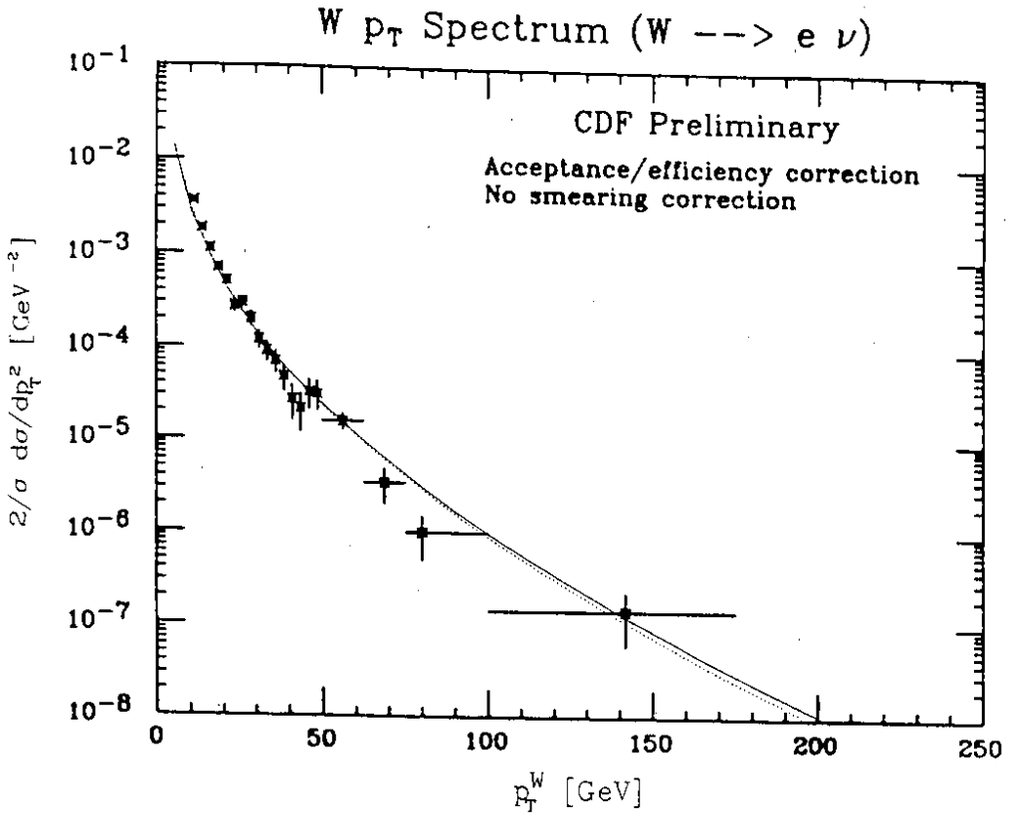
W p_T Spectrum (W --> e ν)
CDF Preliminary
Acceptance/efficiency correction
No smearing correction
$2/\sigma\ d\sigma/dp_T^2\ [GeV^{-2}]$
p_T^W [GeV]

Fig. 2

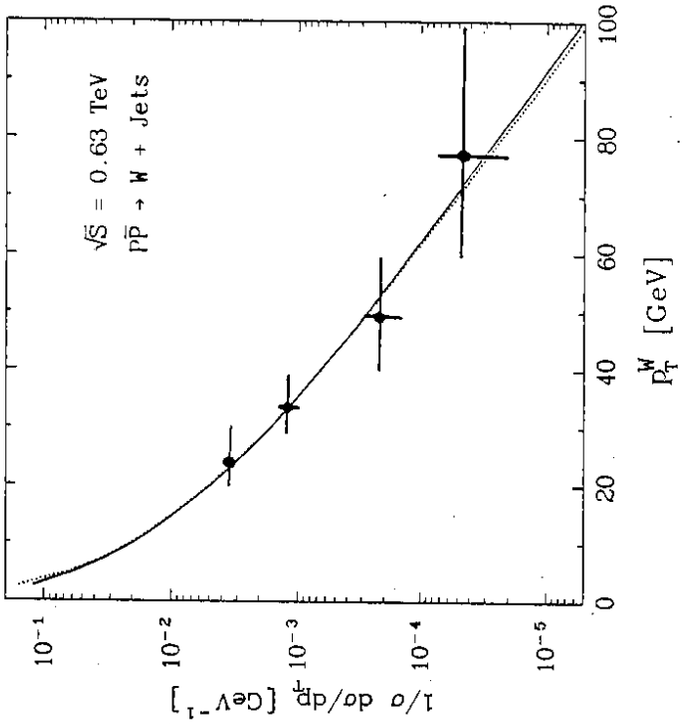
$\sqrt{S}$ = 0.63 TeV
$p\bar{p}$ → W + Jets
$1/\sigma\ d\sigma/dp_T\ [GeV^{-1}]$
p_T^W [GeV]

Fig. 1

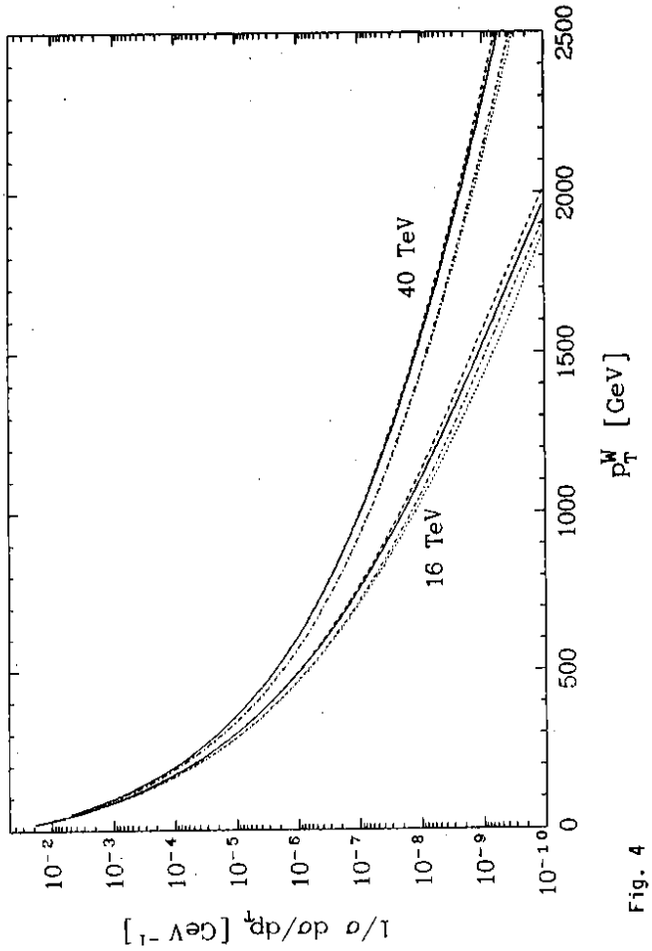

Fig. 4

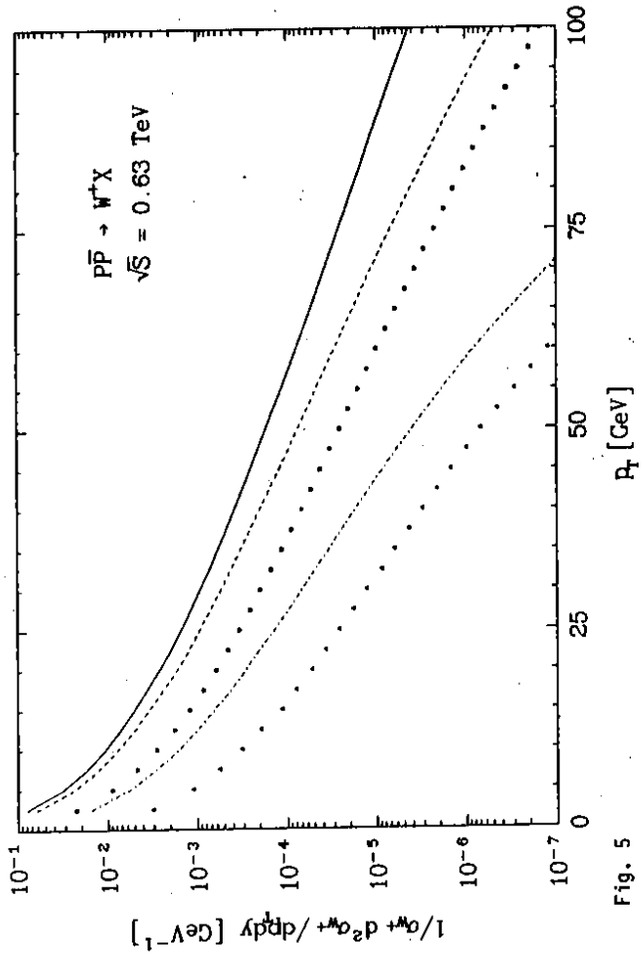

Fig. 5

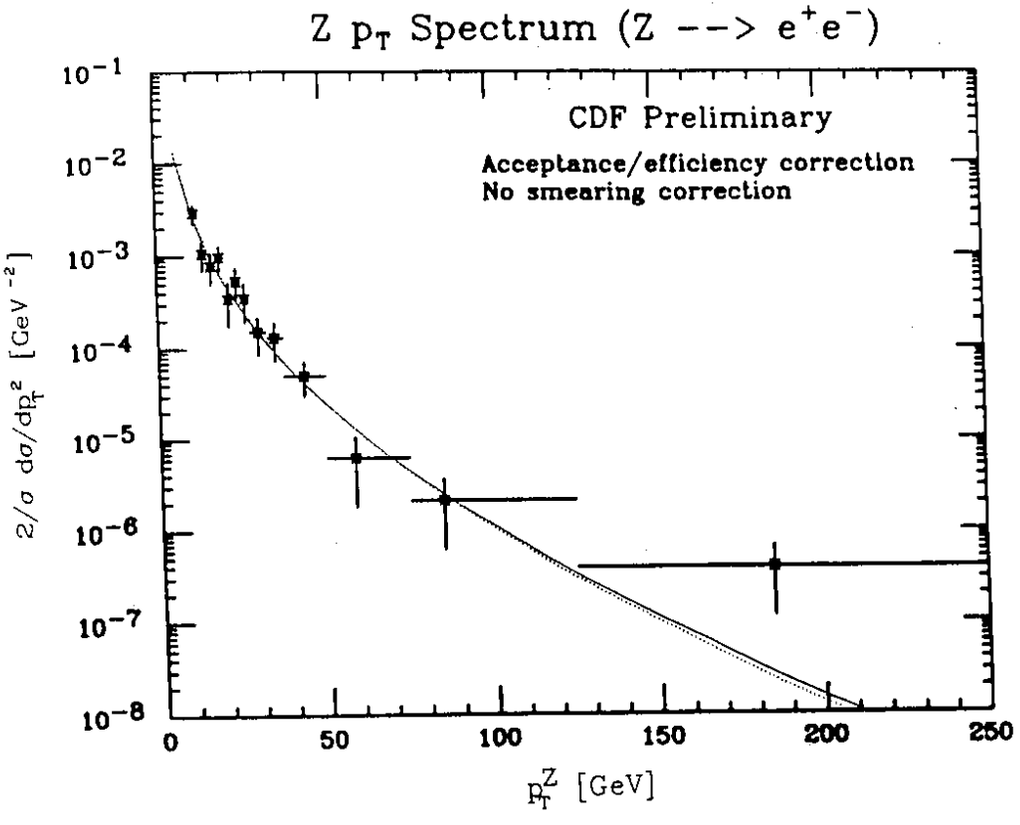

Fig. 3

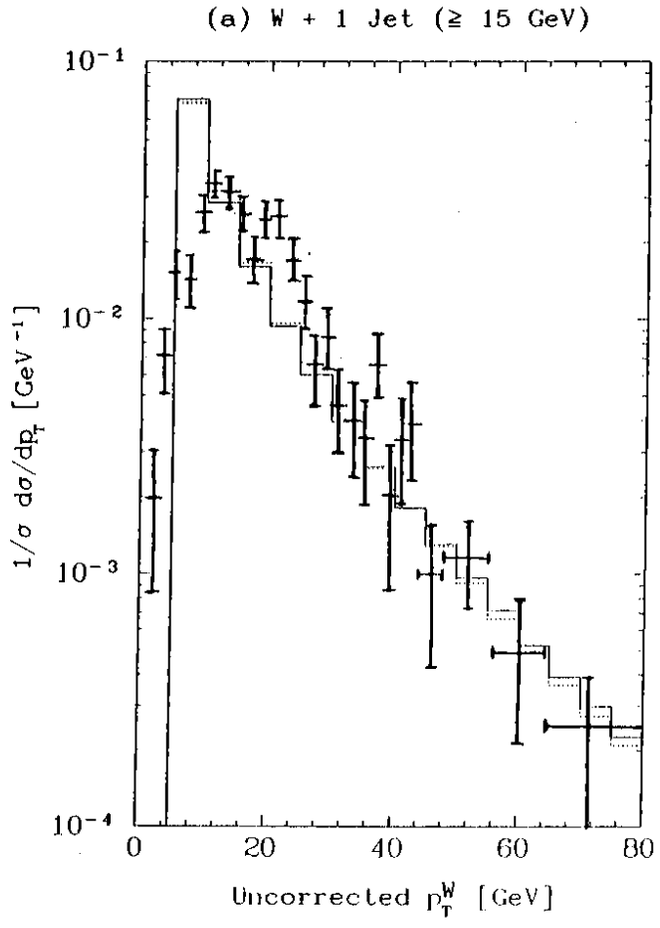

Fig. 8

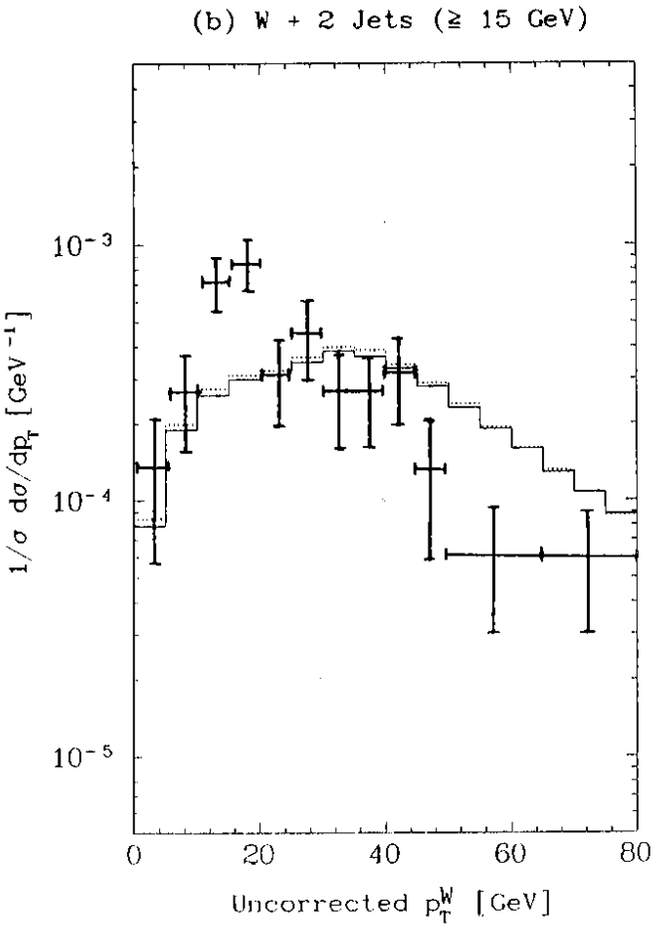

Fig. 9

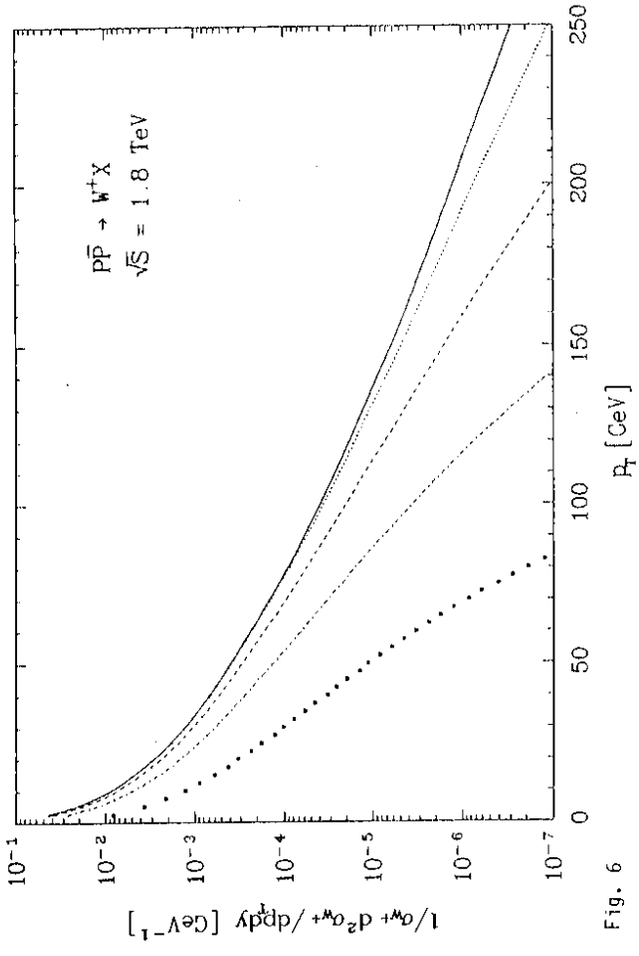

Fig. 6

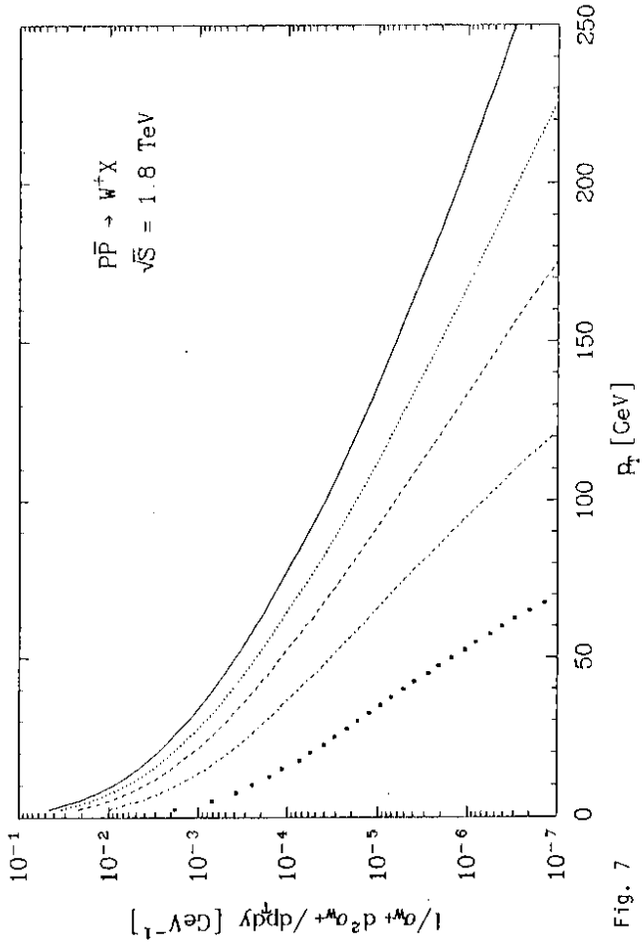

Fig. 7

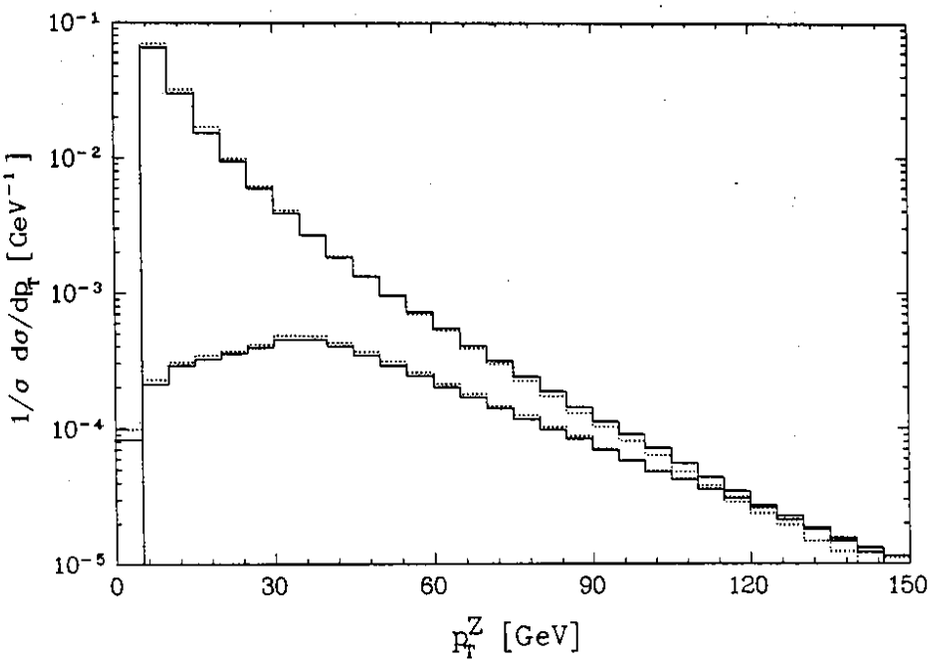

Fig. 10

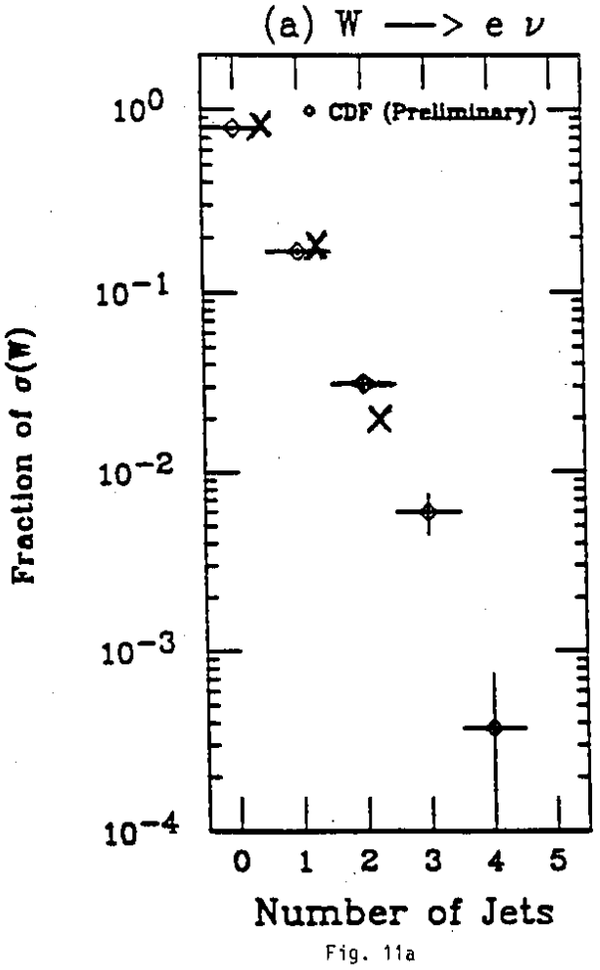

Fig. 11a

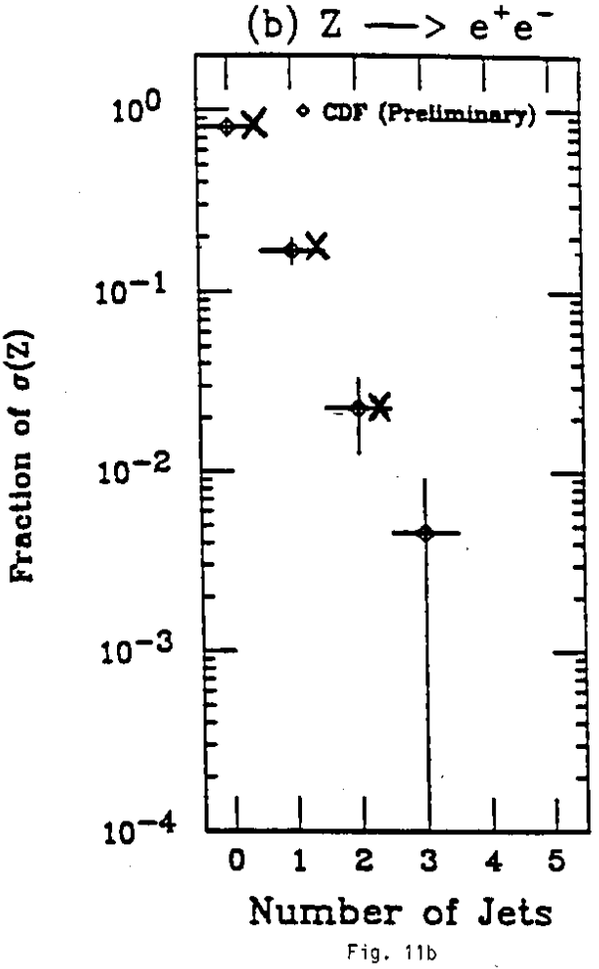

Fig. 11b

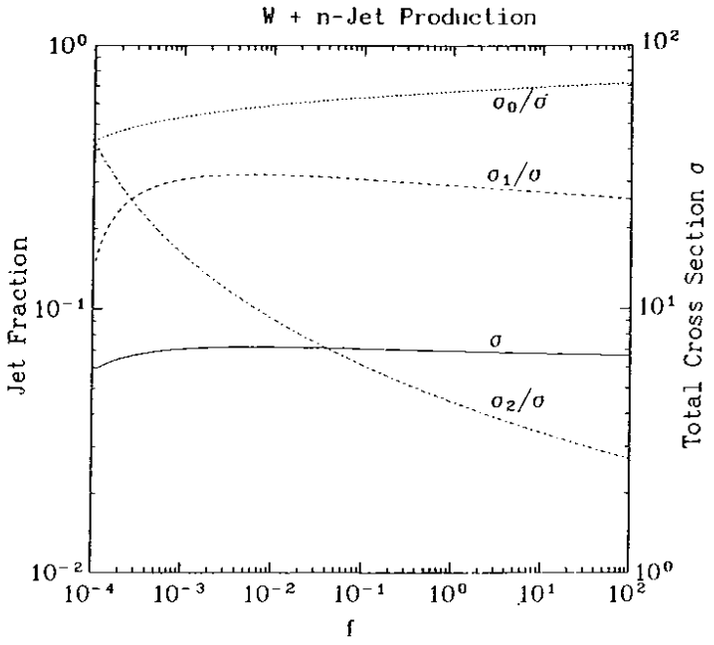
W + n-Jet Production
Jet Fraction
Total Cross Section σ
f
σ0/σ
σ1/σ
σ2/σ
σ

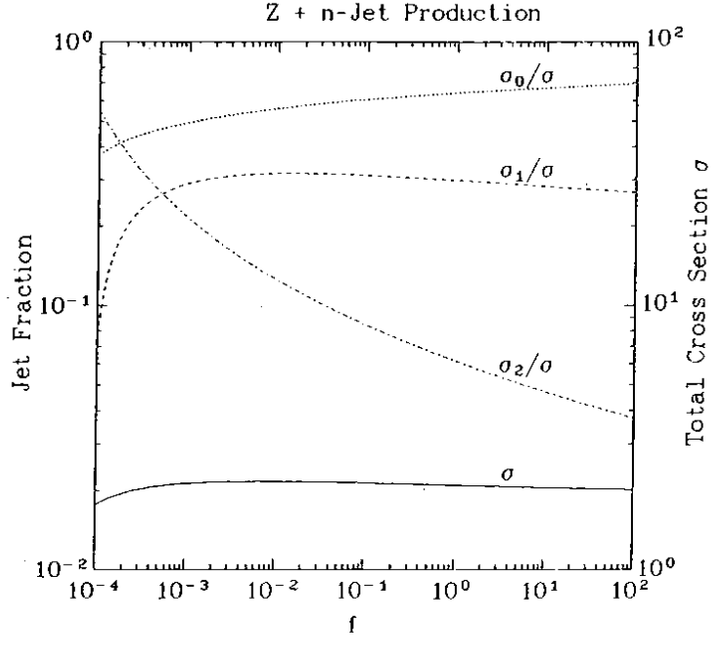
Z + n-Jet Production
Jet Fraction
Total Cross Section σ
f
σ0/σ
σ1/σ
σ2/σ
σ

Fig. 12

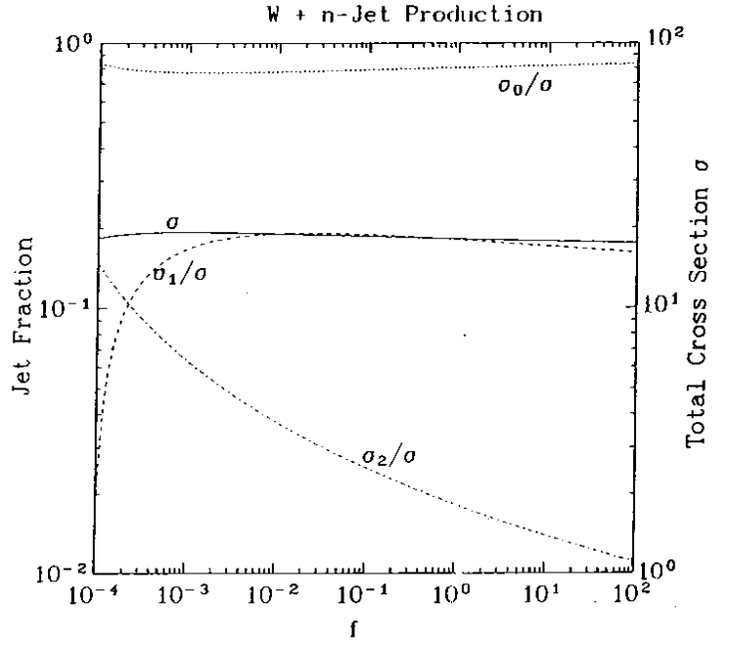
W + n-Jet Production
Jet Fraction
Total Cross Section σ
f
σ0/σ
σ
σ1/σ
σ2/σ

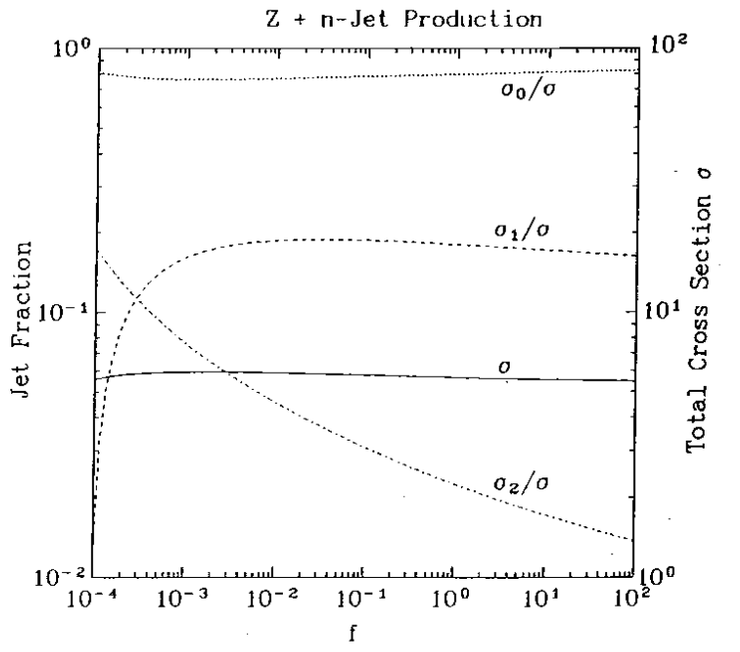
Z + n-Jet Production
Jet Fraction
Total Cross Section σ
f
σ0/σ
σ1/σ
σ
σ2/σ

Fig. 13